Inner-Shell Electron Spectroscopy for Microanalysis

Chemical, structural, and electronic data are obtained by analysis of electron energy losses.

David C. Joy and Dennis M. Maher

Summary. The transmission electron energy-loss spectrum shows characteristic "edges" corresponding to the excitation of inner-shell electrons of atoms in a thin sample. Analysis of these edges provides detailed chemical, structural, and electronic data from the radiated volume. By combining electron spectroscopy and electron microscopy, this microanalytical technique can be performed in conjunction with high-resolution imaging of the sample. It is shown that this approach has advantages of sensitivity, spatial resolution, and convenience over other comparable techniques.

The field of instrumentation and its rapid growth during the past few years have been identified as major factors contributing to many of the recent developments in physics and life sciences (*1*). In this article we discuss a particular example of how instrumental advances have made it possible to put into practice an idea that has been in existence for many years. As long ago as 1944, Hillier and Baker (*2*) suggested that a measurement of the energy spectrum of electrons that have been transmitted through a thin specimen of a material would provide detailed chemical and structural information about the specimen. However, their attempts to demonstrate this technique of microanalysis were hampered by poor electron optics, inefficient electron spectrometers, dirty vacuum systems, and limited data collection facilities. Now, with the benefit of instrumental improvements in three of the areas cited by Weisskopf (*1*), the technique of electron spectroscopy for microanalysis has become a reality.

This has been made possible by the advent of scanning electron probe instruments, efficient electron spectrometers, and convenient, inexpensive computer systems for storage and analysis of data. The scanning electron microscope can form an intense, focused beam of electrons with a diameter of typically 1 to 10 nanometers, which can be positioned on any chosen area of a specimen. With this beam any region of the specimen can be probed for microanalysis, or a high-resolution image can be obtained by scanning the beam over the specimen and displaying the variation in intensity of the transmitted signal on a video monitor. The electrons transmitted through a thin specimen can be analyzed by means of an electron spectrometer, which collects a large fraction of the electrons and disperses them in a focal plane by an amount that depends on their loss of energy relative to the kinetic energy of the incident beam. If the energy-dispersed information is scanned over a selecting slit, an energy-loss spectrum from a specific area of the sample can be obtained.

Recent advances in the design of electron spectrometers (*3*) and a better understanding of how the spectrometer can be coupled efficiently to the electron-optical system (*4*) make it possible to collect energy-loss spectra at a high signal-to-noise ratio from an area of the specimen defined by the diameter of the incident probe. Provided the quality of the vacuum in the microscope is such that irradiating the sample with the electron beam for reasonable time periods does not cause specimen contamination or degradation, spectra can be analyzed in the light of the interactions expected to occur between the incident electrons and the sample. These analyses are performed by use of a computer-based system, which can both store and process the spectral data in order to extract the chemical, electronic, and structural information potentially available. Figure 1 shows a schematic diagram of a combined microscope and microanalytical facility. The ability to perform both imaging and analysis is of importance because it allows the spectral data to be placed in the context of the ultrastructure of the specimen. The combination is an analytic tool of unique capabilities.

Basic Concepts

A system of the type described above can be used to study any of the many possible interactions between an electron beam and a solid specimen, since all generated signals carry information about the solid state. However, much current research interest has been centered on the interactions associated with the excitation of inner-shell electrons. These excitations give rise to a discontinuity or "edge" in the spectrum (see Fig. 2), and edges are of interest because of the diversity of analytical information that can be obtained from them. First, the energy loss at which the edge occurs is a measure of the energy needed to excite an electron from its bound state in the atom. This energy, which is close to the atomic binding energy, is characteristic of the element, and so a determination of the energy loss at which an edge occurs is sufficient to uniquely identify a specific element. Inner-shell excitations are therefore especially suited for elemental microanalysis. Second, the detailed shape of the edge is affected by the chemical state, electronic band structure, and crystallography of the solid in which the atom is situated. A study of these "fine structures" (indicated in Fig. 3) superimposed on the basic profile of an edge can give a detailed picture of the physical environment of the analyzed volume. Third, accurate quantum mechanical calculations of the inner-shell ionization process are now available (*5*, *6*), so the spectral data can be interpreted on the basis of a firm theoretical understanding. Finally, the inner-shell excitation processes are highly localized and therefore suitable for studies at high spatial resolution.

Some of these advantages can, of course, be obtained under other experimental conditions. For example, fluorescent x-rays (*7*) and Auger electrons (*8*) produced in the decay following the primary excitation are widely used for chemical microanalysis. However, in an

---

The authors are members of the Technical Staff, Bell Laboratories, Murray Hill, New Jersey 07974.

0036-8075/79/1012-0162$01.75/0 Copyright © 1979 AAAS

energy-loss experiment it is the primary excitation that is being observed rather than the secondary decay, and therefore the number of analyzable events for a particular incident-beam flux is much higher than for either an x-ray or an Auger measurement. In addition, since the transmitted electron beam is confined within a narrow cone, the geometric collection efficiency of an electron spectrometer optimally coupled to an electron microscope can approach 100 percent (*9*). For x-ray or Auger spectrometers the corresponding figure is closer to 1 percent. The sensitivity of the energy-loss technique is thus higher.

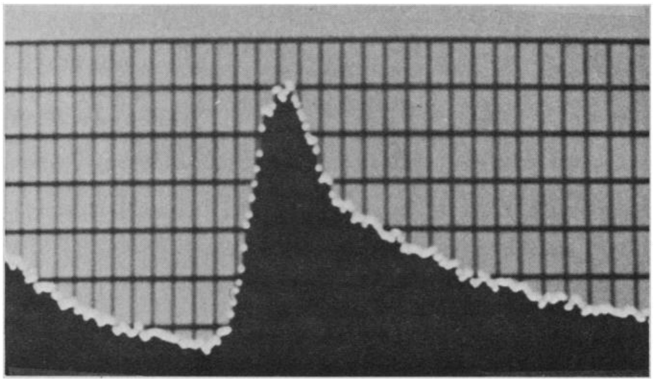

Fig. 2. Part of the energy-loss spectrum from a carbon film, showing the carbon *K* edge. Note the rapidly falling background before the edge, the rapid rise in intensity at the onset of the edge (284 eV), and then the steady decay at higher energy losses.

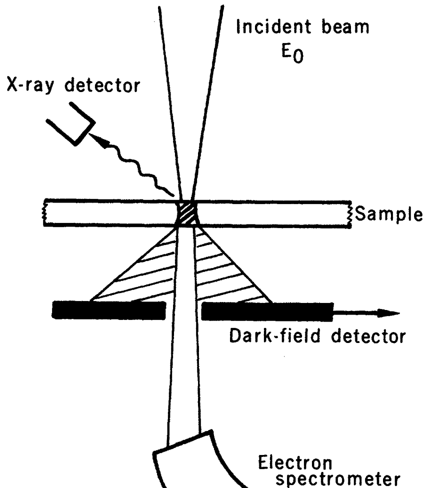

Fig. 1. Schematic illustration of a combined electron microscope and microanalytical facility. The incident beam is focused to a spot (diameter, ≤ 10 nm) on the thin sample (thickness, ≤ 100 nm). While a high-resolution image is recorded with the elastically scattered (dark-field) electrons, the fluorescent x-ray and electron energy-loss spectra can be collected for microanalysis.

Other ways of exciting the inner-shell electrons can be considered. The most important of these is the monochromatic x-ray beam, which has recently come into prominence because of the availability of high-intensity, tunable x-radiation from synchrotron rings (*10*). Surprisingly, even against such competition, a system based on an electron microscope has substantial advantages. This is because the electron beam is a more efficient probe of the structure than is the photon flux from a synchrotron, as can be seen from the following argument (*11*). The number of inner-shell electrons that are excited will determine the sensitivity of a technique for microanalysis. Thus in an electron beam instrument the minimum number of analyzable atoms will be inversely proportional to the particle flux in the incident beam J_E and the ionization cross section $d\sigma/dE$. Therefore a sensitivity factor S_E can be defined as

$$S_E = J_E\, d\sigma/dE \tag{1}$$

Similarly, for the x-ray beam from a synchrotron source, the corresponding sensitivity factor S_X would be

$$S_X = J_X\sigma/\Delta E \tag{2}$$

where J_X is the photon flux per energy width ΔE after monochromatization and σ is the photoabsorption cross section. A figure of merit R between electron beams and synchrotron radiation would then be

$$R = S_E/S_X \tag{3}$$

where a value of R greater than unity indicates higher sensitivity (that is, the ability to detect a smaller number of events or atoms) for the electron beam.

For the inner-shell excitations the ratio of $d\sigma/dE$ to σ at an energy loss E, for incident electrons of energy 100 kiloelectron volts, can be approximated as

$$\frac{d\sigma/dE}{\sigma} \approx \frac{1}{170E}\ln\left(\frac{4 \times 10^5}{E}\right) \tag{4}$$

For example, at the *K*-shell edge of carbon, for which $E = 284$ eV, this ratio is only about 10^{-4}. However, this factor in favor of the photon beam is more than compensated by the difference in the incident flux available in the two cases. Comparing the flux J_E from a typical commercial electron microscope (about 10 amperes per square centimeter) with the photon flux available after monochromatization from the Stanford Proton Electron Accelerating Ring (SPEAR) (*12*) and then calculating the figure of merit R shows that the advantage in favor of the electron beam varies from about 100 to 2 over the range of energy losses 50 to 1000 eV (see Fig. 4, curve a). The latest generation of electron-probe instruments employing cold field-emission sources are capable of current densities up to 10^6 A/cm^2, and these may be comparable to the proposed National Light Source for Brookhaven National Laboratory (*13*) operating at 2.5 GeV. In this case the superiority of the electron-beam device is even higher over the energy-loss range 10 eV to 10 keV.

The significance of this result lies not only in the fact that an electron microscope, even at the state-of-the-art level, is less expensive and more compact than a synchrotron source, but also that the electron flux can be focused into a probe with a very small diameter (tens of angstroms) while the radiation from the synchrotron covers tens of micrometers.

Elemental Studies

The most basic and practical application of electron spectrometry is in elemental analysis of the specimen. In this mode of operation, the energy loss at which an edge can be identified is measured and the intensity contained in this is integrated to quantitate the number of atoms of a specific element present. Thus one is making use of the simplest feature of an edge—the excitation of an inner-shell electron to continuum states. The subtle fine-structure effects that arise because the atoms are assembled into a solid are considered later.

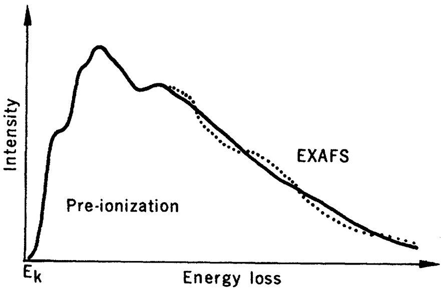

Fig. 3. Diagrammatic representation of a *K* edge after background stripping, showing the threshold (or preionization) fine structure, which extends 10 to 15 eV past the edge onset at E_K, and the extended fine structure, which is detectable for many hundreds of electron volts after the edge.

Figure 5 shows a portion of an energy-loss spectrum recorded from a thin crystal of boron nitride supported on a carbon substrate. The edges in the spectrum correspond to the ionizations of the *K*-shell electrons of boron, carbon, and nitrogen. They are characterized by a sharp rise followed by a gradual decay of the signal on passing through the edge energy. The shape of the *K* edge makes the measurement of its threshold energy relatively easy, and since its threshold energy corresponds very closely to the atomic binding energy, an element can be identified uniquely. Unlike a similar measurement made in ESCA (electron spectroscopy for chemical analysis), which is dependent on the work function of the sample, this measurement is absolute and the identification is therefore positive in almost every case. Within the energy-loss range accessible with a system of the type described here (50 to 2000 eV), *K*-shell edges from the elements lithium to silicon are obtainable. Since these edges are widely spaced (50 to 200 eV), a simple spectrometer with a resolution of 10 eV or better is adequate to resolve them.

Other ionizations, such as those from the *L* and *M* shells, can also be used for microanalysis. However, they differ from the *K* edges in that they do not all display a sharp threshold but instead may have their maximum intensity at an energy loss many electron volts above the threshold. This is because of the centrifugal barrier that must be overcome by an electron excited from an orbit that is not spherically symmetrical. This possibility of a delayed maximum can make a unique identification based on the *L* or *M* edge more difficult, and some additional information, such as the fluorescent x-ray spectrum from the same specimen area, is usually desirable.

A spectrum of the kind shown in Fig. 5 can usually be obtained in 50 seconds in an electron microscope, while still maintaining the standard operating conditions of the instrument. In the particular example shown here, the spectrum was recorded by using a 10-nm probe on a crystal about 50 nm thick, giving a sampled volume of about 10^{-17} cubic centimeter, which corresponds to $\sim 5 \times 10^5$ atoms. A rapid analysis at high spatial resolution is thus possible, particularly for the important elements in the first two rows of the periodic table. The mass sensitivity of the technique is a function of both the element sought and the matrix in which it is set, and Table 1 shows some values we have calculated for elements in a carbon matrix, assuming typical operating conditions. These numbers are in agreement with simplified estimates made earlier (*14*) and values approaching this have been experimentally demonstrated (*9*, *15*).

Table 1. Calculated detectable limits for a carbon matrix. Detectable limits have been calculated for the following conditions: thickness of carbon matrix, 80 nm; E_0, 100 keV; electron flux J, 20 A/cm²-sec; probe diameter, 30 nm; spectrometer resolution, 10 eV; and multichannel analyzer dwell time, 200 msec per electron volt per channel.

Element	Edge	E (eV)	Minimum number of atoms
Lithium	K	55	9.6×10^2
Silicon	L_{23}	99	2.0×10^3
Sulfur	L_{23}	165	3.8×10^3
Boron	K	188	2.9×10^3
Chlorine	L_{23}	201	4.5×10^3
Calcium	L_{23}	348	1.8×10^4
Nitrogen	K	402	1.7×10^4
Oxygen	K	532	2.4×10^4
Fluorine	K	685	3.4×10^4

Although these figures are very encouraging, two difficulties that are often encountered with samples of practical interest must be mentioned. Figure 6, a spectrum from fluorodopamine in synaptosomes (*16*), demonstrates both of these problems. First, in a system where many elements are present there is an overlap between edges because each edge has a substantial natural width. An edge therefore rides on a background determined by the tails of the edges that precede it, and this both reduces the visibility of the edge and lowers the detection sensitivity. Second, if the sample is allowed to become too thick, there is a finite possibility that the incident electron will interact more than once with the sample before it leaves. This plural scattering reduces the visibility of an edge because it is convoluted with the other interactions that have occurred. In the limit, the edge may become no more than a change in slope in the general background intensity of the spectrum. In order to avoid this it is necessary to keep the sample thickness below one mean free path for inelastic scattering. To a fair approximation the total cross section for inelastic scattering at 100 keV is (*17*)

$$\sigma_i \sim 10^{-3}Z^{1/2} \ln\left(\frac{8 \times 10^6}{Z}\right) \mathring{A}^2 \text{ per atom} \tag{5}$$

(where Z is atomic number) so that for light elements such as carbon the mean free path $\lambda = 1/N\sigma_i$ (where N is the number of atoms per unit volume of the sample) is several hundred angstroms. This is less than the thickness of samples normally used for conventional electron microscopy at this voltage, and so very careful specimen preparation is required. While this is not a major problem for the examination of metallic or semiconductor specimens, it is a real problem for biological specimens, since conventional techniques such as ultramicrotomy yield sections that are too thick. Our experience so far has been that sections subjected to minimum handling (that is, unfixed or freeze-substituted) and then cryo-ultramicrotomed are best suited for these studies. Another practical solution is to use electrons of a higher incident energy, such as 200 keV, which gives a nearly proportional gain in usable thickness. Suitable commercial instruments operating at this accelerating voltage are now being fitted with electron spectrometers.

Like most microanalytical techniques, energy-loss analysis is not "trace sensitive," since under any condition the mass of an element in the irradiated volume must exceed the minimum detectable mass. When the probe size is very small this implies that the element of interest must be localized—for example, in a precipitate or inclusion—and consequently the energy-loss technique is ideally suited for the study of such features. However, if the element is distributed homogeneously, then, depending on the concentration, it may be necessary to probe a relatively large volume in order to exceed the detectable limit. It should also be noted that in the case of biological materials there is an upper limit to the electron dose that can be accepted by the specimen before loss of mass, crystallinity, and so on, becomes too great. For a typical proteinaceous material this limit can be as low as 10 electrons per square angstrom, which, for a 100-second analysis period, corresponds to an incident flux of only 10^{-4} A/cm². This, of course, worsens proportionally the mass sensitivity of the technique. However, we have found that under some special conditions—for example, when the material is enclosed by a membrane (in a whole cell or platelet)—the rate of radiation damage can be very much lower, and this offers hope that some solution can be found to this problem. As an example, studies of fluorodopamine incubated with human blood platelets have demonstrated no loss of intensity in the fluorine *K* edge after a dose of 10^3 electrons per square angstrom, even though the same material, outside the cell, yields no edge at even a tenth of this dose (*18*).

Considerable progress has been made

in the quantitation of edge profiles for elemental analysis. Unlike x-ray or Auger techniques, which require correction or standardization procedures to give numerical data, the quantitation of energy-loss spectra is both simple and absolute. The number of atoms per unit area contributing to the observed edge intensity is

$$N = \frac{I_K(\beta,\Delta)}{I_0(\beta,\Delta)\sigma(\beta,\Delta)} \tag{6}$$

where $I_K(\beta,\Delta)$ is the edge signal, after subtraction of the background, integrated over some energy range Δ and for a collection angle into the spectrometer of β measured at the specimen; $I_0(\beta,\Delta)$ is the corresponding signal measured at the zero-loss peak of the spectrum; and $\sigma(\beta,\Delta)$ is the appropriate partial cross section for the ionization event (*19*). The use of computer-based data collection systems has made it a simple matter to model and then remove the background intensity beneath an edge and therefore obtain both I_K and I_0 from the stored spectrum in a direct way. Theoretical developments (*20, 21*) have made it possible to rapidly and accurately calculate partial cross sections under conditions that correspond to those found in practice, making possible a standardless quantitation. We have recently shown that, for the *K* shells, an absolute accuracy of 10 percent for N in boron nitride can be obtained in this way, for an analyzed mass of the order of 10^{-17} gram (*22*).

Although this spectral analysis technique is useful for many purposes, a practical limitation is set by the fact that the spectrum is sequentially recorded, and thus considerable time is needed to obtain an adequate signal-to-noise ratio for any part of the spectrum. To examine the spatial distribution of a particular element would therefore require substantial time. This can be avoided by changing the mode of operation of the analyzer.

If the spectrometer is adjusted so that electrons showing a particular energy loss, such as a *K*-shell loss for an element of interest, as passed through the selecting slit of the analyzer, then the detected signal will vary depending on whether the chosen element is present in the volume examined. In the absence of the element the signal will be the local background intensity for that energy loss, while in the presence of the element the signal will be increased by an amount that depends on the quantity of the element in the irradiated volume. Thus in the scanning transmission microscope a display of the spectrometer output will give an image whose brightness is an indication of the presence or absence of the selected element, and a distribution can be mapped rapidly. Because the background intensity itself can vary from point to point in the specimen when the mass-thickness of the section changes, it is necessary to have a way of distinguishing chemical effects from mass-thickness variations (*23*). This is readily done by recording images from the same area at energy losses just below, and then just above, the chosen edge. Thickness changes will cause the same contrast effects in both images, but specific elemental contrast will be visible only in the image taken above the edge.

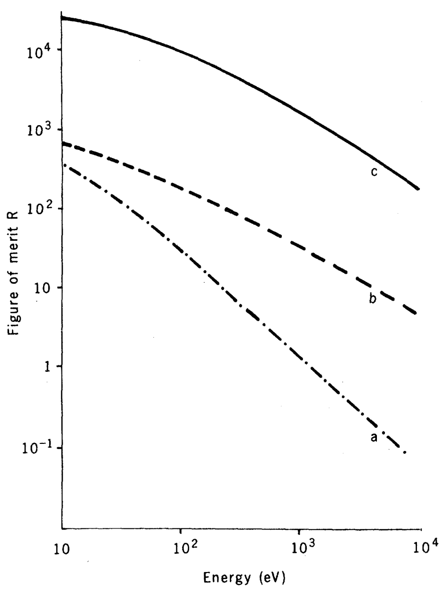

Fig. 4. Comparison of relative detection sensitivities for electron and photon beam systems, where *R* is defined in Eq. 3. (Curve a) A conventional 100-kilovolt electron source producing 10 A/cm^2 at the sample is compared with the present performance of SPEAR (*12*), assuming 1-milliradian acceptance by the electron spectrometer. (Curve b) The same systems are compared but a spectrometer acceptance of 20 mrad is assumed. (Curve c) A 100-kV field-emission source producing 10^6 A/cm^2 at the sample is compared with the proposed Brookhaven National Light Source (*13*), assuming a spectrometer accepting 20 mrad.

This technique has been applied to a variety of problems (*15, 24, 25*), in both materials science and biology. A particularly useful application has been to the study of the distribution of biologically active groups at a subcellular level. This has been done by replacing one or more of the hydrogen atoms in the group of interest with fluorine and then mapping the fluorine distribution by the method outlined above. Because these fluorine analogs usually behave very similarly to the original group and because in most living systems little or no fluorine is naturally present, this approach has proved very successful (*15*). Figure 7 shows an example in which the distribution of serotonin within human blood platelets has been mapped by using a 4-fluoro analog of serotonin (*26*). The images taken below and above the fluorine *K* edge show clearly the contrast due to the presence of fluorine and hence reveal the location of the serotonin within the platelet (*27*). Techniques of this kind have been applied to study the distribution of other groups such as cholesterol and glucose, and recent experiments have shown that as little as 10 percent fluorine by weight is needed to provide adequate mapping.

Threshold Fine Structure:

Electronic and Chemical-State Effects

The profile of an edge reflects not only transitions of inner-shell electrons to high-energy states in the continuum but also discrete transitions to unoccupied states just above the Fermi level. Therefore in a narrow energy range (10 to 15 eV) above the threshold energy of the edge, structure can be resolved. This threshold (or preionization) fine structure represents, in part, the energy and momentum dependence of the density of unoccupied states characteristic of condensed atoms (that is, the band structure of the solid), although in an energy-loss experiment the result is actually a convolution of the initial and final densities of states. If the initial state is relatively simple, as is the case for *K* and *L* shells of light elements, then the observed threshold structure can be attributed predominantly to available unoccupied states in the neighborhood of a specific atom (*28-36*).

In the language of the chemist, these transitions are to low-lying bonding and antibonding orbitals. The interpretation of their π and σ character, in general, has been based on either molecular orbital (*28, 36*) or band structure (*31-33*) calculations. Recent experiments (*35, 37*) have indicated that valuable information about the final-state character can be obtained by studying the momentum dependence of the threshold fine structure. This has been verified for the cause of hexagonal boron nitride (*38*), where it has been shown that the momentum dependence of the boron *K* threshold structure, from crystals with their *c* axes tilted 45° to the incident beam, leads to an unambiguous experimental determination of the $1s \rightarrow \pi^*$ and σ^* antibonding character and energy dependence of the final states. These results are similar to those obtained with polarized electromagnetic radiation (39) and are the first demonstration that a study of this type can be carried out with fast electrons and a microscope.

Since the bonding of the valence electrons in the solid will produce a small change in the local atomic potential, the binding energies of the inner-shell electrons will be altered. This effect is the so-called chemical shift, which was first introduced by Pauling in the 1930's and is well known in photoelectron spectroscopy, where shifts of as much as 5 eV in the binding energy have been reported (40). Therefore, both the chemical shift (reflecting the initial density of states) and the band structure (representing the final density of states) can be utilized to obtain information on the localized chemical state (28, 29, 34, 36). To illustrate this point we cite experiments by Ritsko *et al.* (34), who studied the threshold fine structure of three edges from the one-dimensional organic metal TTF-TCNQ, namely the sulfur L_{23} edge, which is localized in the TTF molecule, the nitrogen K edge, which is localized in the TCNQ molecule, and the carbon K edge, which is common to both. Comparison of the observed energy dependence of the threshold fine structure with calculated energy levels led the authors to conclude that charge transfer between the two molecules was complete (that is, TTF^+ and $TCNQ^-$ were present); there was no evidence for the presence of neutral molecules, which had been predicted from photoemission experiments (41). Although this scattering experiment was not done in an electron microscope, the result is important in relation to both techniques and materials, because the structure of TTF-TCNQ consists of two distinct one-dimensional arrays of donor and acceptor molecules with conduction bands of similar width, and it had not been possible to differentiate between the two conducting paths by other techniques.

Lastly, we note that threshold "anomalies" due to the collective response of the free-electron gas to the sudden creation of an inner-shell "hole" have been observed (37). The result is a sharpening or rounding of the threshold profile, but the detection of these many-body effects requires an energy resolution of 0.1 eV or better, and so in the context of spectroscopy in an electron microscope they usually will not be resolved.

The application of threshold fine-structure effects to materials diagnostics on a micrometer or submicrometer scale is still in its infancy. Nevertheless, there is sufficient evidence from electron microscopy studies (spatial resolution, 10 nm to 1 μm) (28, 29, 31, 38), as well as from inelastic electron spectroscopy in so-called electron scattering chambers (spatial resolution, ~ 200 μm) (35, 36) and x-ray absorption studies with synchrotron radiation (spatial resolution, ~ 1 mm) (42), to indicate that systematic model experiments involving the same atom in different structural or bonding conditions will result in "fingerprints" that can be used for submicrometer analyses of the structural and chemical state of unknowns. The new generation of commercial microscope systems, combining electron spectrometers of sufficient resolution to observe these effects (1 eV or better) with high-brightness electron sources, should enable this promise to be fulfilled.

Extended Fine Structure: Local Atomic Environment

A continuum of transitions to free-electron-like states occurs for energy losses E greater than about 20 eV above the onset of an edge and this continuum extends over hundreds of electron volts. The ejected photoelectrons have a kinetic energy $E - E_B$, where E_B is the inner-shell binding energy, and are therefore characterized by a wavelenth $\lambda = 1.226/(E - E_B)^{1/2}$ nm, which is typically 0.1 nm. Although these electrons experience elastic interactions with neighboring atoms, inelastic processes limit their mean free path to typically 0.5 to 1 nm, so that they travel only a few interatomic distances. Clearly these electrons only explore the local environment of a specific (ionized) atom, and the results of this are revealed through extended intensity oscillations which ride on top of the continuum energy losses.

This extended electron loss fine structure (EXELFS) (30, 35, 43, 44) is equivalent to extended x-ray absorption fine structure (EXAFS), which was first identified in a series of papers by Kronig in the 1930's (45). As a result of considerable theoretical and experimental work over the last 6 years, the interpretation of EXAFS and the data analysis methods leading to quantitative results are quite well developed (46). The extended oscillations are a final-state interference effect between the electron wave from the ionized atom and the diffracted waves from neighboring atoms. These waves can interfere either constructively or destructively, depending on the total phase shift between waves, and this produces maxima and minima on top of the contin-

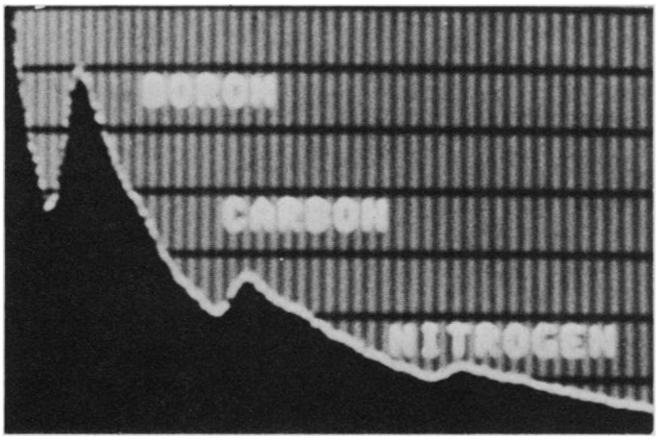

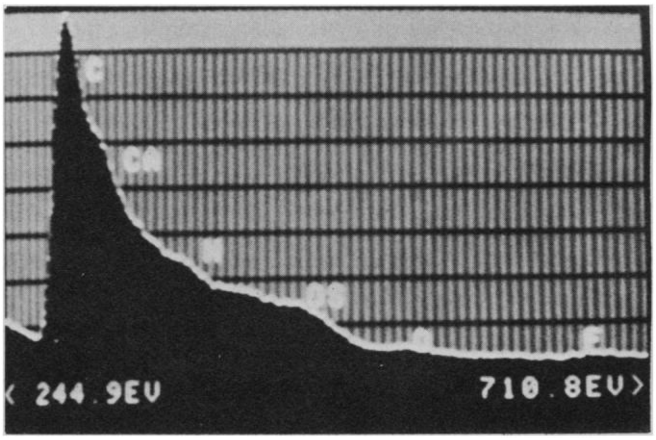

Fig. 5 (left). Portion of the spectrum from a thin crystal of boron nitride supported on a carbon substrate. The spectrum was obtained in 50 seconds from a volume of about 10^{-17} cm^3 (containing about 10^5 atoms) in a standard electron microscope. The K edges from boron (188 eV), carbon (284 eV), and nitrogen (402 eV) are visible. Fig. 6 (right). Part of the spectrum from fluorodopamine in freeze-substituted synaptosomes (16), showing edges from calcium, nitrogen, osmium, oxygen, and fluorine on the tail of the carbon K edge. The number of different edges and the thickness of the sample alter the edge shapes and result in poor visibility.

uum energy-loss spectrum. The amplitude of these oscillations depends on the number N_j and type of atoms in each neighboring shell, thermal and static disorder, and the mean free path of the ejected electron. The frequency of the oscillations is determined by the interatomic distances R_j and the wavelength of the ejected electron (that is, the energy loss) and is modified by the total phase shift.

The experiment is designed to evaluate R_j and N_j. In the general case, this is a difficult task because of the number of variables involved and the correlations between these variables (*46*). Curve-fitting techniques are used to extract the oscillations, and a Fourier transform of these oscillations then results in a radial distribution function for a specific atom. This function isolates the contribution from each shell, and it peaks, depending on the effect of the phase shift, at approximately the atomic positions (typically within ± 0.01 nm). The Fourier amplitudes fall away as $1/R_j^2$ so that, in general, the near neighbors make the dominant contribution. Lastly, the areas under the peaks are, to a first approximation, proportional to N_j/R_j^2 and therefore relative values of N_j can be estimated directly from the transformed data. In the case of x-ray absorption spectra, nearest-neighbor distances have been determined with an accuracy of ±0.001 nm, but this degree of accuracy requires that the phase shifts be evaluated from either a suitable standard (*46*) or theory (*47*). The structural arrangements of a wide variety of materials have been investigated successfully through EXAFS and as few as 10^{13} atoms characterized with a spatial resolution of several millimeters.

The first explicit demonstration of EXELFS in the context of an electron microscope was reported in 1976 by Leapman and Cosslet (*44*), who compared the extended fine structure above the aluminum *K* edge from pure Al and Al_2O_3 and found that the estimated nearest-neighbor distances were in agreement with the x-ray data to within ± 0.01 nm. In these experiments the spatial resolution was about 0.5 micrometer, raising the possibility of micrometer and submicrometer EXELFS studies. The first fully quantitative analysis of EXELFS was reported by Kincaid *et al.* (*35*), who studied the carbon *K* edge in graphite. The first three shells were well resolved, and by using theoretical phase shifts for carbon it was possible to determine the nearest-neighbor distances to an accuracy of ± 0.002 nm. In this case the experiments were performed in an electron scattering chamber (*48*) so that the spatial resolution was ~ 250 μm. Most recently EXELFS has been identified and quantitatively analyzed from as few as 10^4 atoms of carbon in graphite (*49*). These data were obtained in a scanning transmission microscope with a cold field-emmission gun, a probe diameter in the range 1.5 to 10 nm, and collection times as short as 4 minutes. This probably represents the lower limit to what can be achieved in this area since, even with the high brightness of the field-emission gun, the counting statistics are barely adequate to allow the low-level (5 percent) EXELFS modulations to be studied at a high enough signal-to-noise ratio.

In the near future, extended fine-structure measurements at the micrometer level should become routine in materials characterization with the electron microscope. Because the EXELFS modulations for near-neighbor shells are separated by tens of electron volts, they can readily be resolved by simple spectrometers of the kind most easily fitted to a microscope, and in fact the best signal-to-noise ratio will be obtained for resolutions of the order of several electron volts. It may thus be possible to conduct spatially resolved EXELFS experiments for the important elements from lithium to silicon whose *K* edges are not readily accessible by synchrotron-stimulated EXAFS.

Concluding Remarks

The potentials of inner-shell electron spectroscopy in the context of a scanning transmission electron microscope should be clear from this review article. If an incident probe of 10 nm is used and a typical specimen thickness is 50 nm, then the volume analyzed is of order 10^{-17} cm^3, which usually corresponds to 10^5 to 10^6 atoms. The result is therefore a micro-area analytical technique for probing the chemical, electronic, and structural state of a particular element (atom) in an environment of many elements (atoms). Because an image can be formed, the spectral data are related directly to the ultrastructure of the specimen and this combination is a powerful tool for materials characterization and diagnostics.

There has been considerable activity in this field over the past several years and significant number of fundamental studies of the physics of inner-shell excitations have been reported. The availability of commerical electron microscopes that are fitted with an electron spectrometer, whose output is recorded into and processed directly in a multichannel analyzer interfaced to a small computer, will certainly stimulate activity in a broad range of scientific and technological research areas. Of particular interest in this regard is the possibility of conducting in situ experiments where lo-

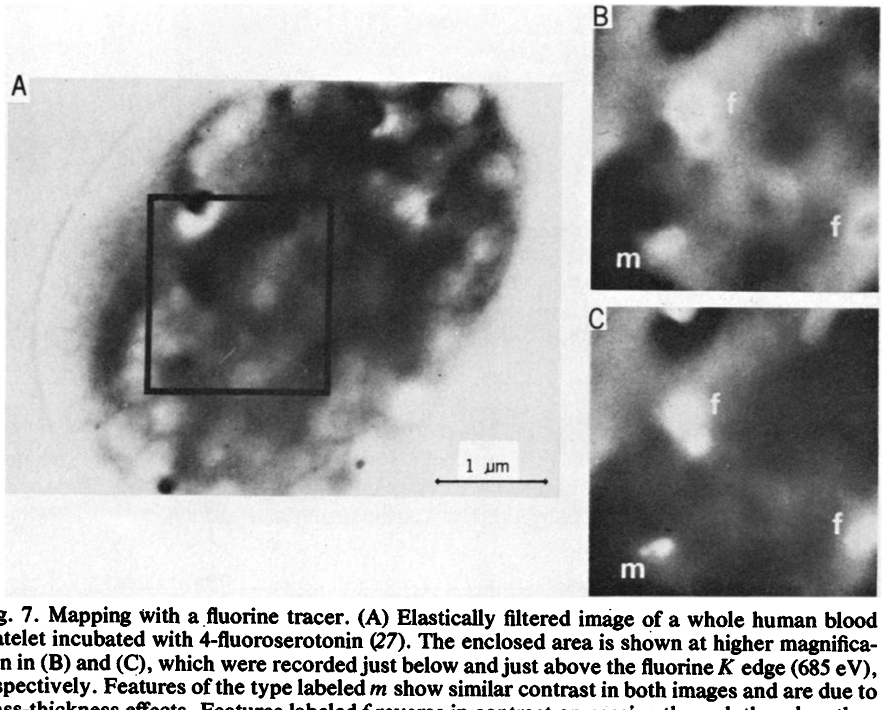

Fig. 7. Mapping with a fluorine tracer. (A) Elastically filtered image of a whole human blood platelet incubated with 4-fluoroserotonin (*27*). The enclosed area is shown at higher magnification in (B) and (C), which were recorded just below and just above the fluorine *K* edge (685 eV), respectively. Features of the type labeled *m* show similar contrast in both images and are due to mass-thickness effects. Features labeled *f* reverse in contrast on passing through the edge; they are due to the presence of fluorine and hence show the location of the serotonin. Comparison with (A) shows that the fluorine-rich areas are correlated with some of the electron-dense areas in the elastic image.

cal chemical, electronic, and structural changes are monitored in situ as a function of imposed environmental conditions. These types of studies may well be the trend in the distant future; however, in the near future it is anticipated that the bulk of the studies will be on model systems in order that the full potential of quantification can be assessed.

References and Notes

1. V. F. Weisskopf, *Science* **203**, 240 (1979).
2. J. Hillier and R. F. Baker, *J. Appl. Phys.* **15**, 663 (1944).
3. See, for example, A. V. Crewe, N. Isaacson, D. E. Johnson, *Rev. Sci. Instrum.* **42**, 411 (1971); J. R. Fields, *Ultramicroscopy* **21**, 311 (1977).
4. A. V. Crewe, *Optik* **47**, 299 (1977).
5. S. T. Manson, *Phys. Rev. A* **6**, 1013 (1972).
6. R. D. Leapman, P. Rez, D. Mayers, *Proc. 9th Int. Congr. Electron Microsc.* **1**, 526 (1978).
7. D. C. Joy and D. M. Maher, *Proc. 10th Annu. Scanning Electron Microsc. Symp.* **1**, 325 (1977).
8. J. A. Venables and A. P. Janssen, *Proc. 9th Int. Congr. Electron Microsc.* **3**, 280 (1978).
9. M. Isaacson and D. E. Johnson, *Ultramicroscopy* **1**, 33 (1975).
10. R. E. Watson and M. L. Perlman, *Science* **199**, 1295 (1978).
11. M. Isaacson and M. Utlaut, *Optik* **50**, 213 (1978).
12. See the data in (*11*) and also in K. O. Hodgson and S. Donach, *Chem. Eng. News* **56**, 26 (21 August 1978).
13. J. P. Blewett, Ed., *Brookhaven Natl. Lab. Rep. BNL 50595* (1977).
14. C. Colliex and P. Trebbia, in *Biological X-ray Microanalysis by Electron Beam Excitation*, C. Lecheme and R. Warner, Eds. (Academic Press, New York, 1979).
15. J. L. Costa, D. C. Joy, D. M. Maher, K. L. Kirk, S. W. Hui, *Science* **200**, 537 (1978).
16. This sample of synaptosomes containing fluorodopamine was prepared by freeze substitution and supplied by J. L. Costa.
17. M. Isaacson, in *Proceedings of a Specialist Workshop on Analytical Electron Microscopy*, J. Silcox and M. Isaacson, Eds. (Materials Research Center, Cornell University, Ithaca, N.Y., 1977), p. 66.
18. J. L. Costa, D. M. Maher, D. C. Joy, unpublished data.
19. R. F. Egerton, *Proc. 11th Annu. Scanning Electron Microsc. Symp.* **1**, 13 (1978).
20. R. D. Leapman, *Ultramicroscopy* **3**, 413 (1978); see also (*5, 6*).
21. R. F. Egerton, in *Proceedings of a Specialist Workshop on Analytical Electron Microscopy*, P. L. Feyes, Ed. (Report 3082, Materials Research Center, Cornell University, Ithaca, N.Y., 1978), p. 232.
22. D. C. Joy, R. F. Egerton, D. M. Maher, *Proc. 12th Annu. Scanning Electron Microsc. Symp.* **2**, 817 (1979).
23. C. Jeanguillaume, P. Trebbia, C. Colliex, *Ultramicroscopy* **3**, 237 (1978).
24. D. C. Joy and D. M. Maher, in *Advances in Electron Microscopy and Analysis*, D. L. Misell, Ed. (Institute of Physics, London, 1978), p. 69.
25. J. L. Costa, D. C. Joy, D. M. Maher, in preparation.
26. K. I. Kirk, *J. Heterocyclic Chem.* **13**, 1253 (1976).
27. These images, of air-dried human blood platelets incubated with fluoroserotonin, are from unpublished work; they are reproduced here by courtesy of S. W. Hui and P. Ottensmeyer.
28. M. Isaacson, *J. Chem. Phys.* **56**, 1813 (1972).

→ D. E. Johnson, *Radiat. Res.* **49**, 63 (1972).

30. C. Colliex and B. Jouffrey, *Philos. Mag.* **25**, 191 (1972).
31. R. F. Egerton and M. J. Whelan, *J. Electron. Spectrosc. Relat. Phenom.* **3**, 232 (1976).
32. ______, *Philos. Mag.* **30**, 739 (1976).
33. C. Colliex, in *Seminar-Bencht Kontron, Analytische Elektronenmikroskopie* (Kontron, Munich, 1976), p. 204; see also C. Colliex, V. E. Cossiet, R. D. Leapman, P. Trebbia, *Ultramicroscopy* **1**, 301 (1976).
34. J. J. Ritsko, N. O. Lipari, P. C. Gibbons, S. E. Schnatterly, *Phys. Rev. Lett.* **37**, 1068 (1976).
35. B. M. Kincaid, A. E. Meixner, P. M. Platzman, *ibid.* **40**, 1296 (1978).
36. J. J. Ritsko and R. W. Bigelow, *J. Chem. Phys.* **69**, 4162 (1978).
37. S. G. Slusky, P. C. Gibbons, S. E. Schnatterly, J. R. Fields, *Phys. Rev. Lett.* **36**, 326 (1976).
38. R. D. Leapman and J. Silcox, *ibid.* **42**, 1361 (1979).
39. J. Kessler, *Polarized Electrons* (Springer-Verlag, New York, 1976).
40. For example, see K. Siegbahn *et al.*, *ESCA Applied to Free Molecules* (North-Holland, Amsterdam, 1969), p. 104.
41. F. Donoyer, R. Comis, A. F. Garito, A. J. Heeger, *Phys. Rev. Lett.* **35**, 445 (1975).
42. P. E. Eisenberger, in *Proceedings of the Robert A. Welch Foundation Conference on Chemical Research, XIX. Photon Chemistry*, W. O. Milligan, Ed. (Welch Foundation, Houston, 1975), p. 171.
43. J. J. Ritsko, S. E. Schnatterly, P. C. Gibbons, *Phys. Rev. Lett.* **32**, 671 (1974).
44. R. D. Leapman and V. E. Cosslet, *J. Phys. D* **9**, 25 (1976).
45. R. de L. Kronig, *Z. Phys.* **70**, 317 (1931); *ibid.* **75**, 191 (1932); *ibid.*, p. 468.
46. P. Eisenberger and B. M. Kincaid, *Science* **200**, 1441 (1978).
47. P. A. Lee and G. Beni, *Phys. Rev. B* **15**, 2862 (1977).
48. A. E. Meixner and G. S. Brown, *Rev. Sci. Instrum.*, in press.
49. P. E. Batson, in *Proceedings of a Specialist Workshop on Analytical Electron Microscopy*, P. L. Feyes, Ed. (Report 3082, Materials Research Center, Cornell University, Ithaca, N.Y., 1978), p. 31; also see *Ultramicroscopy* **3**, 367 (1978); P. E. Batson and A. J. Craven, *Phys. Rev. Lett.* **42**, 893 (1979).

Precision Optical Testing

James C. Wyant

Summary. Increased performance requirements for modern optical systems have necessitated the development of more precise optical testing techniques. The need for accurate and rapid measurements is being met by the use of laser interferometers, microprocessors to gather test data, and computers to analyze the data and remove errors in the test equipment.

During the 1960's new optical testing techniques began to develop with the introduction of the laser. At that time, also, the computer became important in the analysis of optical testing results. Today, with the introduction of more powerful minicomputers and microprocessors, vast improvements are being made in both the quality of optical testing and the cost. Formerly, large vacuum tanks were required to test large optics so that atmospheric turbulence would not affect the results. Now with the availability of rapid, low-cost data reduction, large optics can be tested many times in the presence of atmospheric turbulence, and the results can be averaged to reduce the effects of turbulence.

Computers are also beginning to play an important role in reducing the quality of accessory optics used in an optical test. Formerly, all accessory optics had to be of better quality than the optics under test. Now it is almost a routine matter to calibrate the quality of accessory optics and subtract the test errors in the data analysis of the test result.

This article first describes classical optical testing techniques, and then the basic interferometric testing techniques, with emphasis on laser techniques. New techniques made possible by the use of computers and microprocessors are also described.

Testing Techniques

Three noninterferometric testing techniques are the Foucault knife-edge test, the Ronchi test, and the Hartmann test. Before looking at these tests, let us look at what an optical test should measure.

Ideally, light coming from a single object point should, after reflection off a mirror or transmission through a lens, be focused to a perfect point. However, because light travels as a wave, it never comes to a perfect point focus, but rather is spread over some area. This spread is known as the point image irradiance distribution. For a perfectly designed and

---

The author is a professor of optical sciences at the Optical Sciences Center, University of Arizona, Tucson 85721.

0036-8075/79/1012-0168$01.00/0 Copyright © 1979 AAAS